ELSEVIER

On the Reduction of the Radar Backscatter by Oceanic Surface Films: Scatterometer Measurements and Their Theoretical Interpretation

Martin Gade, Werner Alpers,* Heinrich Hühnerfuss,† Volkmar R. Wismann,‡ and Philipp A. Lange§*

During the two SIR-C/X-SAR missions in 1994, surface film experiments were performed in the North Sea with a 5-frequency/multipolarization scatterometer flown on a helicopter, in order to investigate the reduction of the radar backscatter in the presence of quasibiogenic and anthropogenic sea surface films, particularly, at different wind speeds. Under all wind conditions encountered in this study, the measured damping ratio (i.e., the ratio of the radar backscatter from a slick-free and a slick-covered water surface) increases with increasing Bragg wavenumber. It is shown that not only Marangoni damping theory, but also wind-induced effects, primarily the energy input by the wind into the wave spectrum, also have to be taken into account. The reductions measured at low to moderate wind speeds (3.5–4 m/s and 5 m/s) are qualitatively explained by means of a comparison of the different source terms of the action balance equation. For the case of high wind speed (12 m/s) a theoretical model for the damping ratios is developed. Using this model, the experimental data can well be reproduced, and the absence of the Marangoni damping maximum at intermediate Bragg wavenumbers (approximately 100 rad/m) can be interpreted. Furthermore, the model can explain the similarities between the radar backscatter reductions measured over quasibiogenic and anthropogenic surface films under high wind conditions. ©*Elsevier Science Inc., 1998*

INTRODUCTION

The damping of short gravity-capillary ocean surface waves by biogenic and anthropogenic surface films consisting of surface-active components and by mineral oil, respectively, is a well-known phenomenon and has been subject of various investigations (Lucassen-Reynders and Lucassen, 1969; Hühnerfuss and Garrett, 1981; Lucassen, 1982; Hühnerfuss, 1986; Ermakov et al., 1986; Alpers and Hühnerfuss, 1988; 1989; Lombardini et al., 1989; Wu, 1989; Wei and Wu, 1992; Frysinger et al., 1992; Onstott and Rufenach, 1992; Hühnerfuss et al., 1994; 1996; Gade et al., 1998a,b,c; Wismann et al., 1998; V. Wismann, personal communication, 1993). At intermediate incidence angles (between 20° and 75°), these surface waves are responsible for the backscattering of microwaves of comparable wavelengths [Bragg scattering, see Valenzuela (1978)] and, thus, wave damping by oceanic surface films causes a reduction of the measured radar backscatter. For this reason, dark patches visible on synthetic aperture radar (SAR) images of the ocean surface can often be related to oil spills or natural slicks floating on the sea surface. However, they can also be caused, for example, by atmospheric effects like wind shadowing or tropical rain cells (see Alpers, 1995; Melsheimer et al., 1998). Taking into account the characteristic shape of

* Institut für Meereskunde, Universität Hamburg, Hamburg, Germany

† Institut für Organische Chemie, Universität Hamburg, Hamburg, Germany

‡ Institute for Applied Remote Sensing, Wedel/Holstein, Germany

§ Bundesanstalt für Wasserbau, Aussenstelle Küste, Hamburg, Germany

Address correspondence to Martin Gade, Univ. Hamburg, Inst. Für Meereskunde, Troplowitzstr. 7, D-22529 Hamburg, Germany. E-mail: gade@ifm.uni-hamburg.de

Received 1 December 1997; revised 10 April 1998.

REMOTE SENS. ENVIRON. 66:52–70 (1998)
©Elsevier Science Inc., 1998
655 Avenue of the Americas, New York, NY 10010

0034-4257/98/$19.00
PII S0034-4257(98)00034-0

Table 1. Parameters of the HELISCAT System[a]

Scatterometer type	Superheterodyne Doppler Scatterometer
Antenna type	Parabolic dish, 96 cm∅
Polarization	HH, HV, VV, VH
Nominal flight altitude (m)	150
Nominal ground speed (m/s)	50
Nominal incidence angle range (°)	23–65
Pulso repetition frequency (kHz)	40

	Radar Band				
	L	*S*	*C*	*X*	*Ku*
Frequency (GHz)	1.0	2.4	5.3	10.0	15.0
Output power (mW)	150	100	40	10	10
Antenna beamwidth (2-way; 3 dB) (°)	17.0	7.1	3.2	1.7	1.1
Minimum/maximum footprint	53.1×24.4	22.0×10.1	9.9×4.6	5.3×2.4	3.4×1.6
Dimensions ($m \times m$)	128.9×37.4	57.7×15.5	23.2×7.0	12.3×3.7	8.0×2.4
Bragg wavenumber range (rad/m)	14.3–38.0	37.7–91.1	86.1–199.8	163.7–380.0	245.5–569.4
Bragg wavelength range (cm)	43.9–16.5	16.7–6.9	7.3–3.1	3.8–1.7	2.6–1.1

[a] The minimum/maximum dimensions of the radar footprint have been calculated assuming incidence angles of 23° and 53°, respectively, which were the minimum/maximum values during the present investigation.

these dark patches automatic slick detection algorithms have recently been developed for using the 5.3 GHz (C band) SAR aboard the European Remote Sensing Satellites (ERS-1 and ERS-2) for operational oil spill surveillance (Wahl et al., 1994; Pellemans et al., 1995).

The thickness of a mineral oil spill is much larger than that of a monomolecular sea slick, which results in different viscoelastic properties and, therefore, in a different damping of the ocean surface waves (see, e.g., Alpers and Hühnerfuss, 1988; 1989). Several experiments have been performed with natural and artificial sea slicks on the open ocean and in laboratory wind wave tank facilities in order to investigate the specific damping behavior of surface-active substances [see Gade et al. (1998b) and literature cited therein]. The results of the laboratory experiments showed that Marangoni damping (Lucassen-Reynders and Lucassen, 1969; Cini and Lombardini, 1978; Alpers and Hühnerfuss, 1989) is the dominant mechanism for the damping of short sinusoidal gravity waves by monomolecular slicks (Hühnerfuss, 1986). Following Marangoni damping theory, monomolecular surface films exhibit a resonancelike damping behavior, whereas this damping maximum is absent for (thick) mineral oil spills.

Since a single-frequency radar system (like the C band SAR aboard the ERS-1) can provide information on the damping of ocean surface waves at only one frequency, multifrequency radar techniques have already been used to obtain more reliable information on the damping behavior of the detected surface films (Bentz, 1980; Singh et al., 1986; Okamoto et al., 1993; Gade et al., 1998b; Wismann et al., 1998; V. Wismann, personal communication, 1993). However, during recent field experiments with artificial monomolecular surface films in the German Bight of the North Sea, a distinct damping maximum at intermediate wavenumbers (of about 100 rad/m) was not measured (V. Wismann, personal communication, 1993; Gade et al., 1998b). This can be explained by means of additional energy fluxes at the water surface, like the energy input by the wind, wave breaking, and nonlinear wave–wave interaction (Hasselmann, 1962, 1963a,b; Phillips, 1977). Thus, additional terms describing the above energy fluxes have to be taken into account for the development of theoretical models which can explain the damping of small ocean surface waves by different surface films.

During the two Spaceborne Imaging Radar C/X band Synthetic Aperture Radar (SIR-C/X-SAR) missions in April and October 1994, surface films of different viscoelastic properties were deployed in the German Bight of the North Sea, in order to simulate different biogenic and anthropogenic ocean surface films. The aim of these experiments was to investigate whether active microwave techniques are capable of yielding information about the damping behavior of 1) surface films of different viscoelastic properties and 2) one surface-active substance under different environmental conditions. SAR images of the surface films were taken from the 3-frequency/multipolarization SAR aboard the space shuttle Endeavour. In parallel, we performed a total of 125 overflights to obtain radar backscatter measurements over the same sets of surface films with a 5-frequency/multipolarization scatterometer flown on a helicopter (called HELISCAT). In this article, we present the results obtained by HELISCAT, whereas the results of the analyses of the SAR images are summarized in Gade et al. (1996, 1998b). In addition, we include data which were obtained by HELISCAT during a second measurement campaign in April 1994, also in the German Bight of the North Sea.

After a description of the HELISCAT system and of the experimental conditions in the next section, the theoretical background is summarized in the third sec-

Table 2. Absolute Values and Phases of the Dilational modulus $E=-|E|\exp(i\theta)$ for the Substances Deployed in the Dedicated Field Experiments[a]

Abbreviation	*Substance*	$\lvert E\rvert$ $(N\ m^{-1})$	θ *(deg)*
OLA	Oleyl alcohol	0.0255	−175
OLME	Oleic acid methyl ester	0.0100	−5
TOLG	Triolein	0.0115	−175

[a] The estimated errors for the absolute values are better than ±20% and for the phases ±2°. For a detailed description of the dilational modulus and the method of measuring both parameters the reader is referred to Hühnerfuss (1986).

tion. The results obtained during the measurement campaigns are presented in the fourth section. The fifth section includes a discussion of the results and a simple model which has been developed in order to explain the measured reductions of the radar backscatter by the surface films at high wind speeds. Finally, a conclusion is given in the sixth section.

EXPERIMENTAL SETUP

HELISCAT System

HELISCAT (HELIcopter SCATterometer) was developed and built at the University of Hamburg and is flown on a Messerschmidt–Bölkow–Blohm BO-105 helicopter. It operates at 1.25 GHz, 2.4 GHz, 5.3 GHz, 10.0 GHz, and 15.0 GHz (L, S, C, X, and Ku band, respectively) and is capable of performing radar backscatter measurements quasi-simultaneously at the four polarization combinations VV, VH, HH, and HV (the first and the second letters denote the polarization of the transmitted and of the received microwave, respectively; V means vertical and H horizontal polarization). HELISCAT uses a single broad-band antenna both for transmission and reception. The antenna is aft-looking and can be tilted mechanically in such a way that the *nominal* incidence angle covers the range between 23° and 65°. The *effective* incidence angle, particularly at L and S band, is smaller than the nominal incidence angle by a few degrees (for the calculation of the effective incidence angle the antenna beam geometry has to be taken into account). By using different radar frequencies and by varying the incidence angle, HELISCAT covers a Bragg wavenumber range (see below) between 16 rad/m and 569 rad/m. The system parameters of HELISCAT are given in Table 1.

Since only the ratio of the backscattered radar power from a slick-free and a slick-covered water surface is of interest in the present investigation (see below), HELISCAT was not absolutely calibrated [thus yielding the relative backscattered power (RBP) instead of the normalized radar cross section (NRCS)]. For the calculation of the mean relative backscatter from slick-free and slick-covered sea surfaces sections of the backscatter time series from each run were taken (each consisting of 20–70 data points, depending on slick dimensions and flight direction). Only data with a signal-to-noise ratio exceeding 3 dB (measured over the slick-covered areas) have been used, in order to avoid any influence of the instrumental noise on the obtained results. The measured damping ratio used in the present investigation is the ratio of the mean relative backscatter from a slick-free and a slick-covered water surface.

Surface Film Experiments

According to the analyses of Hunter and Liss (1981) natural surface films mainly consist of fats, carbohydrates, proteins, sterols, and fatty acids, with a hydrophobic alkyl chain (preferentially with a length between C_{14} and C_{20}) and a hydrophilic head group. Typical of natural surface films are C_{16} and C_{18} components (e.g., Hühnerfuss et al., 1982; Hühnerfuss, 1986); hence, these derivatives were used in the experiments reported herein to produce quasibiogenic surface films.

Quasibiogenic substances, like oleyl alcohol, oleic acid methyl ester, and triolein (abbreviated as OLA, OLME, and TOLG, respectively, see Table 2), form monomolecular surface films which are well suitable to simulate slicks of natural origin. Since the specific damping characteristics of OLA are best known from several former wave damping experiments [see Gade et al. (1998b) and literature cited therein], this substance was used in each of the dedicated experiments, thus allowing to study the dependence of the damping behavior of one particular substance on environmental conditions, particularly on the wind speed.

All surface film experiments reported herein were performed in the German Bight of the North Sea. The first experiment took place on 18 April 1994, between 04:54 UTC and 05:52 UTC, west of the island of Sylt. Before the HELISCAT measurements started, 120 liter OLA were thrown as frozen chunks from a (second) helicopter onto the sea surface. While these chunks were melting, OLA spread on the water surface in such a way that an area of approximately 0.5 km^2 was covered by this quasibiogenic slick. A wind speed of 5 m/s was encountered, a moderate wind speed at which a strong damping by OLA occurs, since Marangoni wave damping is still more important than the wind input. SIR-C/X-SAR images of the OLA slick were acquired at 05:26 UTC (Gade et al., 1998b). The change of the damping behavior within the first minutes after the slick deployment was already investigated by Hühnerfuss et al. (1996); we therefore concentrate herein on the results obtained after the slick was fully spread.

A second experiment was performed on the same day, between 08:31 UTC and 09:56 UTC, northeast of the German island of Heligoland (at a distance of about 70 km from the former test site). Meanwhile, the wind

Table 3. Position of the Dedicated Surface Film Experiments, Environmental Conditions (Wind Speed U_{10}, Air Temperature T_a, Sea Surface Temperature *SST*), and Times for Slick Deployments and Radar Backscatter Measurements[a]

Position	U_{10} *(m/s)*	T_a *(°C)*	*SST (°C)*	*Time/ Deployment (UTC)*	*Substance*	*Time/ Measurement (UTC)*	*Runs*
				18 April 1994, Sylt			
54°54′N; 7°50′E	5	3.3	7	04:15–04:55	OLA (120 L)	04:54–07:52	15
				18 April 1994, Heligoland			
54°17′N; 8°00′E	3.5–4	6.1	7	07:30–08:15	OLA (120 L)	08:31–09:56	18
				6 October 1994, Sylt			
54°58′N; 7°45′E	12	11.0	12	04:40–0645	OLA (220 L)	08:58–09:51	24
					OLME (60 L)		11
					TOLG/p (160 L)		14
					TOLG/d (20 L)		6
					IFO 180 (200 L)		25

[a] Also listed are the deployed substances (see Table 2; the abbreviations TOLG/p and TOLG/d denote triolein deployed as pure and dissolved substance, respectively) and the number of overflights with HELISCAT (runs).

speed had decreased from 5 m/s to 3.5–4 m/s. In addition to an OLA slick (again, consisting of 120 L of oleyl alcohol), four slicks consisting of quasibiogenic substances which were dissolved in the solvents ethanol and *n*-hexane were deployed from a small vessel. An extensive analysis of the results obtained from these slicks was already presented by Hühnerfuss et al. (1996); therefore, only the results obtained from the (pure) OLA slick will be discussed herein.

During the second SIR-C/X-SAR mission on 6 October 1994, another surface film experiment took place west of the island of Sylt. In addition to 220 L of OLA (which were again deployed on the water surface by means of frozen chunks) a total of 180 L triolein (TOLG) and 100 L oleic acid methyl ester (OLME) were deployed both as pure substances (i.e., as frozen chunks) as well as dissolved in solvents ethanol (OLME) and *n*-hexane (OLME and TOLG). Furthermore, 200 L of mineral oil (abbreviated as IFO 180) were deployed from board an oil recovery ship.

The condition of a slick may be readily ascertained since its optical properties are very pronounced when viewed from a high elevation made possible by the helicopter. At the sea surface encountered, we know from past experiments that newly spread films reach an equilibrium state after 30–40 min. Shortly before the shuttle overflight, at about 07:00 UTC, an atmospheric front passed the area so that the wind speed increased from 6 m/s to 12 m/s. Due to a technical defect, HELISCAT measurements could be performed not earlier than 08:58 UTC (and lasted until 09:51 UTC). However, continuous air surveillance conformed that most of the surface films were not yet destroyed (particularly those films consisting of pure substances) and an adequate data set could be obtained. The SIR-C/X-SAR images of the test site taken at 07:12 UTC at L, C, and X band, VV polarization, are shown in Figure 1 (adopted from Gade et al., 1998b).

The experimental conditions, like location and times of slick deployment and HELISCAT measurements, air and sea surface temperature, substances and number of overflights, are listed in Table 3.

BASIC THEORY

Marangoni Damping

The damping of small gravity and gravity-capillary (sinusoidal) water waves by monomolecular surface films can be explained by *Marangoni damping* theory (Lucassen-Reynders and Lucassen, 1969; Lucassen, 1982; Hühnerfuss, 1986; Alpers and Hühnerfuss, 1989). According to this theory, the dependence of the damping ratio $y(k)$, that is, the ratio of the viscous damping coefficients for slick-covered and for a slick-free water surface, Δ_s and Δ_0, respectively, on the wavenumber k of the water surface waves can be approximated by the following expression:

$$y(k)=\frac{\Delta_s(k)}{\Delta_0(k)}=\frac{1+X(\cos\theta-\sin\theta)+XY-Y\sin\theta}{1+2X(\cos\theta-\sin\theta)+2X^2} \qquad (1)$$

with

$$X=\frac{|E|k^2}{\sqrt{2\omega^3\eta\rho}} \qquad Y=\frac{|E|k}{4\eta\omega}.$$

Here $|E|$ and θ denote the absolute value and the phase of the complex dilational modulus $E=-|E|\exp(i\theta)$ of the surface film, respectively, and $\omega=(gk+\tau k^3)^{1/2}$ is the angular frequency of the water surfce waves [for a detailed discussion on the parameters "magnitude and phase of the dilational modulus" the reader is referred to Hühnerfuss (1986)]. The parameters η and ρ denote the dynamic viscosity and the density of the water, respectively, τ is the ratio of the water surface tension and density, and g is the acceleration of gravity. The rheological parameters $|E|$ and θ of the deployed substances were taken from Hühnerfuss (1986) and are summarized in Table 2.

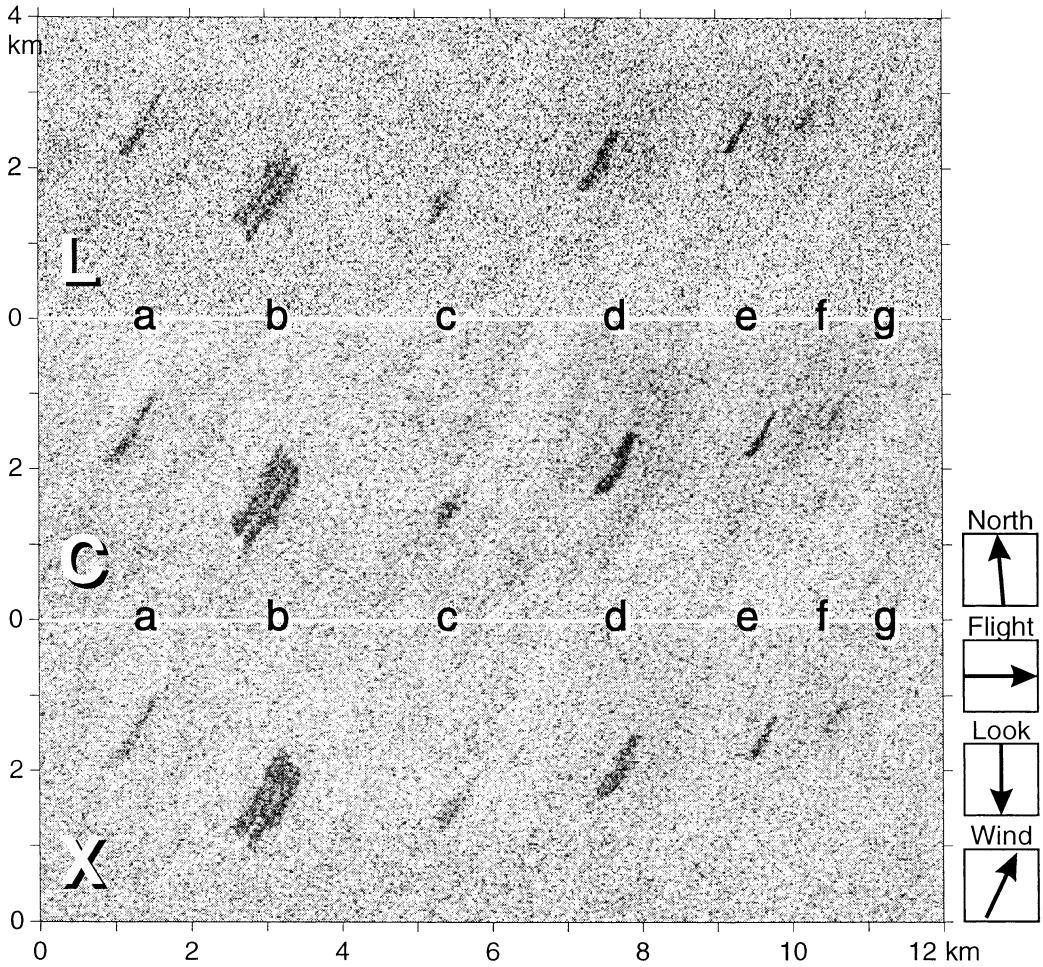

Figure 1. SIR-C/X-SAR images of the second surface film experiment in the German Bight showing surface films consisting of a) IFO 180, b) OLA, c) OLME, d) TOLG, e,f) TOLG and OLME, respectively, spread with the help of *n*-hexane, and g) OLME spread with the help of ethanol. The bright spot at the lower end of the OLA slick is due to an oil surveillance ship. The images were acquired at L-, C-, and X-band, VV polarization, on 6 October 1994, at 07:12 UTC (dimensions 12 km by 4 km). (Images courtesy of NASA and DUR.)

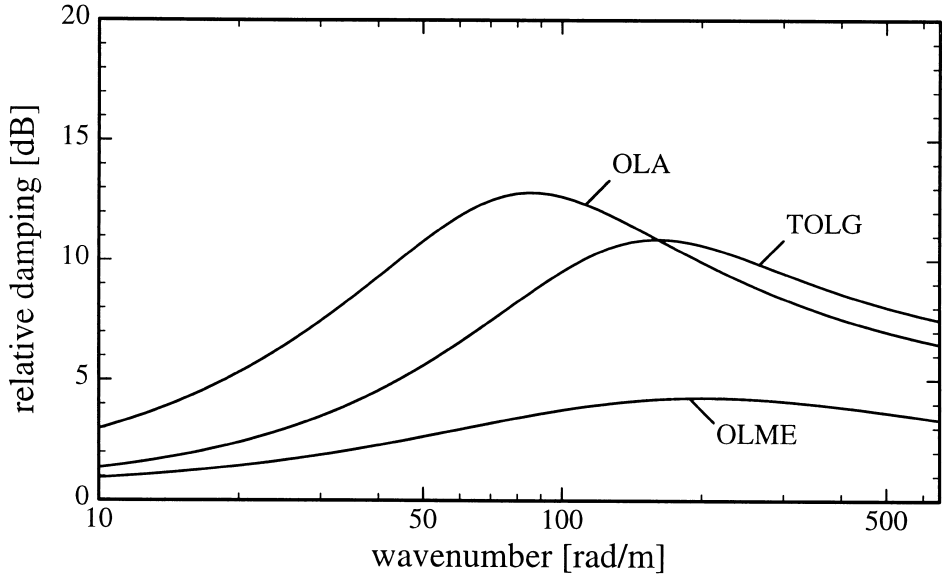

Figure 2. Theoretical damping curves for the deployed substances according to Marangoni damping theory; the parameters of the dilational modulus $E=-|E|\exp(i\theta)$ are given in Table 2.

These parameters were determined by measuring the viscous damping coefficients Δ_s and Δ_0 in wind–wave tank experiments with mechanically generated waves (Hühnerfuss, 1986). Although the resulting damping coefficients are not very exact (and thus the parameters $|E|$ and θ), they are at present the best values to use in our investigation [the relative error of the damping coefficient $y(f)$ is estimated to be better than 20%, which is sufficient for this study]. Inserting these parameters into Eq. (1) and setting $\tau=7.3\times10^{-5}$ m^3/s^2, $g=9.81$ m/s^2, $\rho=1000$ kg/m^3, and $\eta=0.001$ Pa s, the theoretical damping curves shown in Figure 2 were calculated.

Bragg Scattering

During the experiments reported herein, measurements of the radar backscattering were performed at intermediate incidence angles (between 20° and 53°). For these incidence angles, the radar backscattering from the water surface can be described, to first order, by Bragg scattering theory (Wright, 1968; Valenzuela, 1978). According to this theory, the normalized radar cross section (NRCS) is proportional to the spectral energy density of the Bragg waves, that is, of those surface waves of wavenumber k_B that obey the Bragg resonance condition

$$k_B=2k_0 \sin \vartheta, \tag{2}$$

where k_0 denotes the radar wavenumber and ϑ the incidence angle. For a slick-free water surface the NRCS σ_0 can be written as

$$\sigma_0=T_{ij}\cdot\Psi(\pm k_B) \tag{3}$$

with

$$T_{ij}=|g_{ij}|^2 16\pi k_0^4 \cos^4 \vartheta,$$

where $\Psi(\pm k_B)$ is the spectral power density of the Bragg waves with wavenumber k_B. The function $|g_{ij}|^2$ depends on radar wavenumber, dielectric constant ε of the water, incidence angle, and polarization (ij=HH, VV, HV, and VH). The thickness of a surface film (either a monomolecular slick or a thin oil spill) is small compared with the penetration depth of microwaves into the water; therefore, we may assume that the Bragg coefficient T_{ij} is not affected by the presence of a thin surface film, that is,

$$T_{ij}^{(0)}\approx T_{ij}^{(s)}, \tag{4}$$

where the superscripts (0) and (s) denote a film-free and a film-covered water surface, respectively. For an explicit expression of T_{ij} the reader is referred to, for example, Valenzuela (1978).

Source Terms in the Action Balance Equation

One of the goals of the present experiments was to investigate the influence of environmental conditions (particularly of the wind speed) on the damping characteristics of the same substance (OLA). The impact of the wind speed on the damping behavior can be explained by means of the corresponding source term in the action balance equation (Hasselmann, 1962; 1963a,b):

$$0=\frac{dN}{dt}=S_{wi}+S_{nl}-S_{vd}-S_{br}, \tag{5}$$

where $N=\omega/k\cdot\Psi$ is the spectral action density of the water surface waves, and S_{wi}, S_{nl}, S_{vd}, and S_{br} are the source terms of energy input by the wind, by nonlinear wave–wave interaction, and of energy loss by viscous dissipation and wave breaking, respectively. An expression for the source term of viscous dissipation can be found, for example, in Phillips (1985) as

$$S_{vd}^{(i)}=2\Delta_i c_g\cdot N_i(k), \tag{6}$$

where c_g is the group velocity of the water waves and $i\in\{0;s\}$. The viscous damping coefficient for a slick-free water surface, Δ_0, can be found, for example, in Phillips (1977):

$$\Delta_0=\frac{\Delta k^2\eta\omega}{\rho(g+3\tau k^2)}. \tag{7}$$

Using Eqs. (1) and (7), the viscous damping coefficient for a slick-covered water surface, Δ_s, can be expressed as $\Delta_s=y(k)\cdot\Delta_0$. The source term for the wind input was given, for example, by Plant (1982) and Mitsuyasu and Honda (1982):

$$S_{wi}^{(i)}=\beta^{(i)}\cdot N_i(k), \tag{8}$$

with

$$\beta_i=M(\cos\varphi)^{2p}\left(\frac{u_*^{(i)}}{c}\right)^2\omega,$$

where φ is the angle between the wind and wave direction, u_* is the wind friction velocity, and c is the phase velocity of the water waves. The parameters M and p are usually set to 0.04 and 0.5, respectively (Plant, 1982). The friction velocity on a slick-free water surface, $u_*^{(0)}$, can be set as 3.5% of the wind speed, U_{10} (Wu, 1975).

In laboratory measurements, Mitsuyasu and Honda (1982) found that the coverage of the water surface by a surface film causes reductions of the friction velocity by up to 32%. In similar experiments, Gade et al. (1998a) found reductions between 35% and 52% (the differences between both results may be due to a different experimental setup and to the application of different chemical compounds). During field experiments with natural surface films, Wei and Wu (1992) measured reductions of the friction velocity between 3% and 16%. During the SAXON-FPN campaign in 1990, a reduction of the friction velocity of 30% due to an OLA slick was measured (S. Stolte, personal communication, 1991). Since these experimental conditions were most comparable to those of the experiments reported herein, we assume an average reduction of the friction velocity by about 30%, that is, Eq. (9):

$$u_*^{(s)} = 0.7 \cdot u_*^{(0)}. \quad (9)$$

Combining Eqs. (3), (5), (6), and (8), we obtain the following expression for the damping ratio, that is, the ratio of the normalized radar cross sections of a slick-free and a slick-covered water surface,

$$\frac{\sigma_0^{(0)}}{\sigma_0^{(s)}} = \frac{\Psi_0(k)}{\Psi_s(k)} = \frac{N_0(k)}{N_s(k)} = \frac{\beta_s - 2\Delta_s c_g}{\beta_0 - 2\Delta_0 c_g} \cdot \frac{S_{nl}^{(0)} - S_{br}^{(0)}}{S_{nl}^{(s)} - S_{br}^{(s)}}. \quad (10)$$

Using the results obtained in the present experiments, we will show that, under high wind conditions (U_{10}>10 m/s), the damping ratio can successfully be simulated by taking into account also the source term of wave breaking. However, we will first use Eq. (10) for some qualitative analyses.

RESULTS

In this chapter the results of the three experiments performed with HELISCAT in April and October 1994 are presented. On 18 April 1994, we performed measurements not only with pure OLA slicks. However, for the aim of the analyses presented herein, only data obtained from these slicks are used. A detailed discussion of the remaining data set can be found in Hühnerfuss et al. (1996).

Damping Ratios of OLA at Moderate Wind Speed (5 m/s)

On 18 April 1994, radar backscatter measurements were performed at moderate wind speed (5 m/s) over a monomolecular surface film consisting of OLA. Overflights over the slick-covered water surface took place in such a way that the (aft-looking) antenna was looking upwind, downwind, or crosswind (i.e., the flight direction relative to the wind direction were parallel, antiparallel, or orthogonal, respectively). The measured damping ratios are shown in Figure 3. In panel a the data are discriminated by antenna look direction and in panel b by radar polarization. For a better visualization we have refrained from including error bars; however, the calculated errors usually are better than 3 dB. The horizontal bars added into both panels (and in any of the following plots of the measured results) denote the Bragg wavenumber ranges covered by the different radar bands of HELISCAT (see Table 1).

The scatter of the data is large, and it is obvious that no significant dependence of the measured damping ratios was observed for antenna look direction or for radar polarization. Furthermore, no distinct damping maximum at intermediate Bragg wavenumbers, as predicted by Marangoni damping theory (see Fig. 2), was measured.

Damping Ratios of OLA at Low Wind Speed (3.5–4 m/s)

A second experiment was carried out on 18 April 1994, again, with a monomolecular surface film consisting of OLA. The measured damping ratios determined in the presence of this slick at low wind speed (3.5–4 m/s) are depicted in Figure 4. Again, no significant dependence was found for antenna look direction (not shown herein) or for radar polarization (see Fig. 4).

For Bragg wavenumbers lower than about 80 rad/m the damping ratios are comparable to those measured at moderate wind speed (see Fig. 3). However, at high Bragg

Figure 3. Damping ratios as a function of Bragg wavenumber measured by HELISCAT over the OLA slick at moderate wind speed (5 m/s). The data are sorted by antenna look direction relative to the wind direction (panel a) and by the polarization (panel b). The horizontal bars at the bottom of each panel denote the Bragg wavenumber coverage by the different radar bands [see Eq. (2) and Table 1].

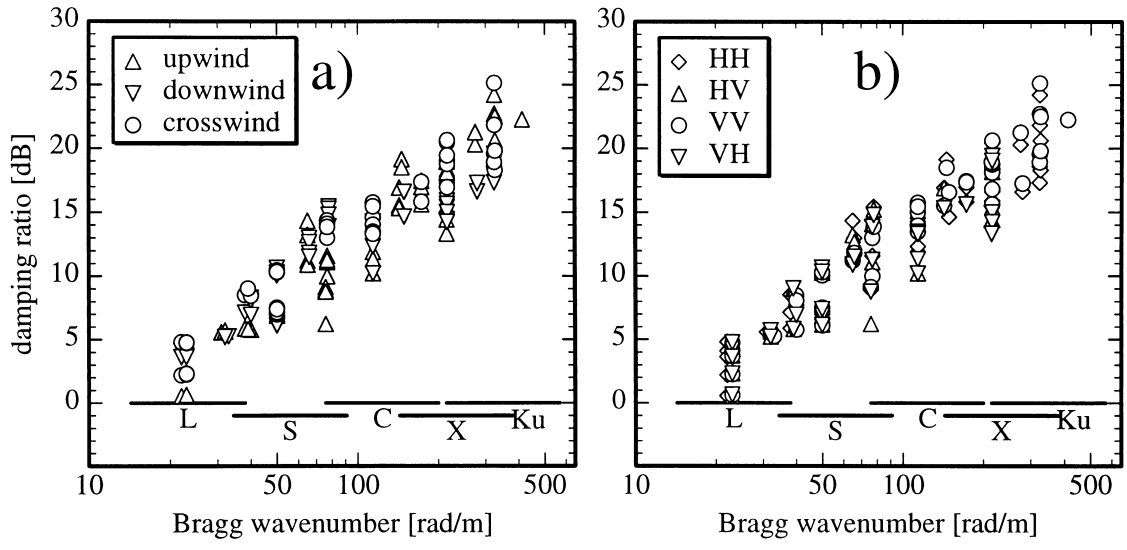

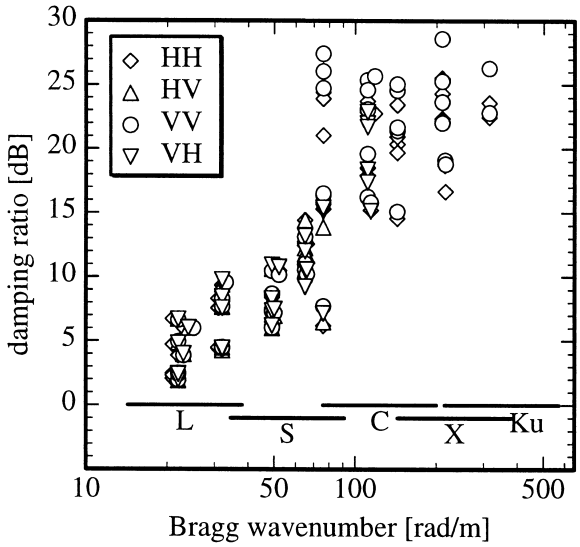

Figure 4. Same as Figure 3, but the damping ratios were measured at low wind speed (3.5–4 m/s).

wavenumbers (k_B>80 rad/m), we measured a stronger damping of the radar backscatter than in the previous experiment (e.g., at moderate wind speed the maximum measured damping ratios at k_B=200 rad/m are less than 20 dB, whereas they are almost 30 dB in the case of low wind speed). Moreover, the scatter of the data is also increased at high Bragg wavenumbers.

Damping Ratios of Various Substances at High Wind Speed (12 m/s)

The experiment on 6 October 1994 took place at high wind speed (12 m/s). Under these conditions (and, particularly, taking into account that the measurements were performed more than 2 h after the slick deployment), we cannot assume that all of the slicks on the water surface were still coherent. Thus, the measured data exhibit a large scatter, depending on the part of the (meanwhile elongated) slicks which was overflown by the helicopter. In order to overcome any difficulties in explaining the measured results, we subdivided the data into classes of different (maximum) damping, that is, the data set of each overflight (run) was related to one of the damping classes "strong," "medium," and "weak," depending on the maximum damping ratio measured during this overflight. We are aware that this discrimination, particularly the chosen limits between the different damping classes, is arbitrary. However, it can be assumed that only in the "strong" damping parts were the surface films not disrupted, whereas in the "medium" and even "weak" damping parts (small) holes may have been produced by the action of wind and waves. Thus, a classification must be made, in order to allow for a comparison with the above results obtained during the former experiments. Again, no significant dependence was found for antenna look direction or for polarization for the whole data set obtained during these measurements.

The results for the OLA slick are shown in Figure 5. The solid line denotes theoretical values which were calculated using the model described in the next chapter. Directly before the SIR-C/X-SAR images were taken, an oil recovery ship sailed through the OLA slick (see Fig. 1). Therefore, this slick was additionally tattered which results in a strong scatter of the measured damping ratios shown in Figure 5 (particularly of the "weak" damping parts shown in panel c). Three damping classes were defined (i.e., "strong," "medium," and "weak"; see panels a, b, and c, respectively) with limiting (maximum) damping ratios of 20 dB and 15 dB. The "strong" damping parts (with a maximum damping above 20 dB) show a monotonic increase in the damping ratios which is in accordance with the above presented results for OLA. However, we measured lower damping ratios than for the cases of moderate and low wind speed, particularly at high Bragg wavenumbers (see Figs. 3 and 4, respectively). The backscatter reductions measured over the "medium" damping parts (panel b) also show a monotonic increase in the damping ratios with Bragg wavenumber. For the "weak" damping parts (panel c) an increase in the damping ratios was measured only at low Bragg wavenumbers (up to about 90 rad/m), whereas no increase in the damping ratios was found at intermediate and high Bragg wavenumbers (k_b>90 rad/m).

The results for the OLME slick are shown in Figure 6 (the solid line corresponds to theoretical values calculated with the model described below). Only two damping classes were chosen, because of the overall low damping capabilities of OLME (see the theoretical damping curves shown in Fig. 2). The measured damping behavior is comparable to that of OLA (Fig. 5): A monotonic increase in the damping ratios was measured over the "strong" damping parts, whereas the "weak" damping parts show no increase at intermediate and high Bragg wavenumbers.

The two surface films consisting of OLME dissolved in solvents ethanol and *n*-hexane, respectively, had already disappeared from the water surface when the HELISCAT measurements started. Thus, no results for these particular slicks could be obtained.

Two surface films consisting of TOLG (deployed as pure substance and dissolved in *n*-hexane) had been deployed on 6 October 1994. At the beginning of the HELISCAT measurements (08:58 UTC), both surface films could clearly be located and, therefore, damping measurements could be performed over both slicks (however, only the pure TOLG slick remained on the water surface for the whole measurement period).

The results for the pure TOLG slick are shown in Figure 7 and those for the dissolved TOLG in Figure 8. Both were subdivided into the three classes "strong,"

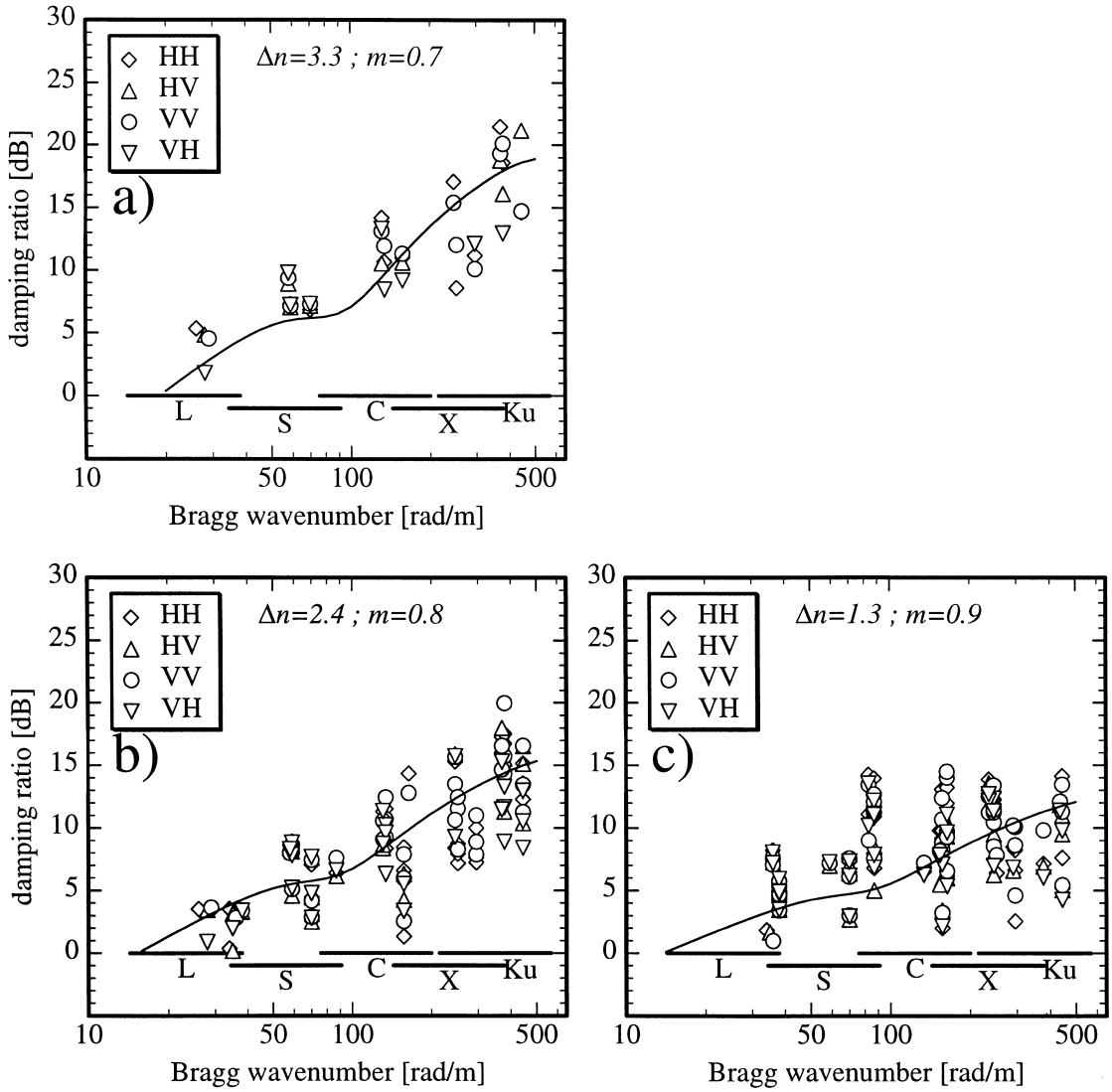

Figure 5. Same as Figure 3, but the damping ratios were measured at high wind speed (12 m/s). The total of data is subdivided into "strong" damping (panel a: maximum damping ratio larger than 20 dB), "medium" damping (panel b: maximum damping ratio between 15 dB and 20 dB), and "weak" damping (panel c: maximum damping ratio up to 15 dB). Theoretical damping curves calculated using Eq. (15) are added into each panel. The parameters m and Δn (describing the reduction of the friction velocity and of the wave breaking, respectively; see text) are also inserted.

"medium," and "weak" damping, corresponding to maximum damping ratios of more than 15 dB (panels a), between 10 dB and 15 dB (panels b), and less than 10 dB (panels c), respectively. The two surface films consisting of TOLG show the same qualitative damping behavior in the "strong" damping parts (although fewer data were obtained over the slick consisting of dissolved TOLG): As already shown for OLA and OLME the damping ratios are increasing with Bragg wavenumber (see panels a of Figs. 7 and 8). Both data sets obtained over the "weak" damping parts of the TOLG slicks (panels c of Figs. 7 and 8) show comparably small damping ratios with a larger scatter for the slick consisting of pure TOLG.

Finally, the results obtained from the mineral oil (IFO 180) film are shown in Figure 9 (again, the limiting damping ratios were chosen as 20 dB and 15 dB). In all three cases (i.e., for the "strong," "medium," and "weak" damping parts) the damping ratios increase monotonically with Bragg wavenumber, i.e., no kink at intermediate Bragg wavenumbers was measured. No constant damping ratios at intermediate to high Bragg wavenumbers were observed over the "medium" and "weak" damping parts (see panels b and c of Fig. 9). The "strong" damping parts caused the highest damping ratios measured during this experiment (almost 30 dB at Ku band, see panel a of Fig. 9).

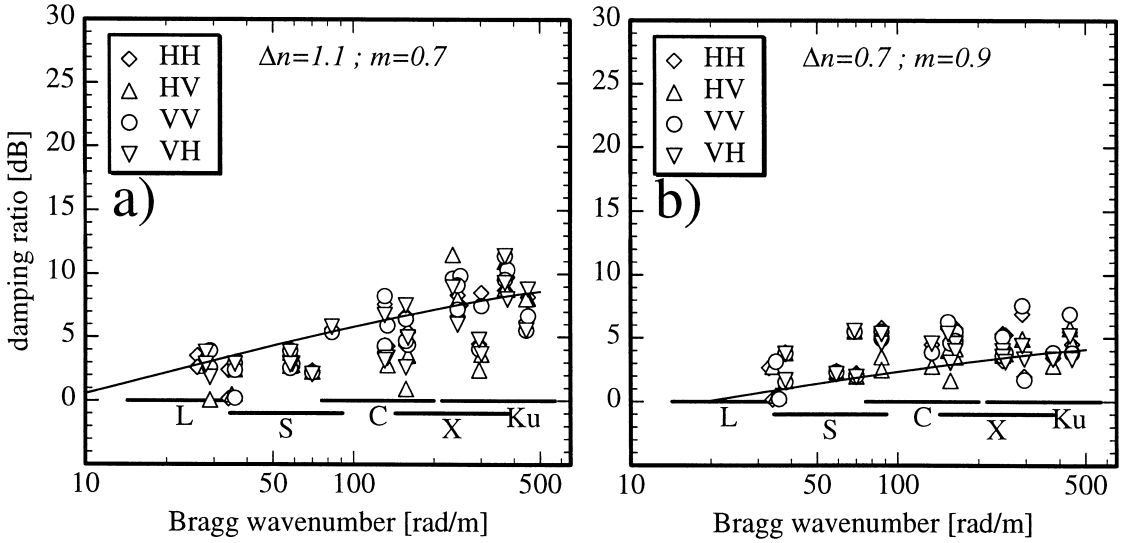

Figure 6. Same as Figure 5, but for OLME. The limit for the discrimination between "strong" and "weak" damping (panels a and b, respectively) is 10 dB.

DISCUSSION

During the three experiments on 18 April and 6 October 1994, a large data set was obtained by HELISCAT. In the first section of this chapter we qualitatively discuss the measured damping ratios, primarily concentrating on 1) the wind speed dependence of the damping behavior of the OLA slicks and 2) the comparison of the damping ratios measured for the different surface films at high wind speed (12 m/s). A simple model is developed for the high wind speed case, in order to explain the measured damping ratios, particularly the absence of the Marangoni maximum.

Qualitative Discussion of the Measured Damping Ratios

Measurements with HELISCAT were performed over OLA slicks under different environmental conditions (see Table 3): First, the air and water temperatures were different and, second, the wind speed varied (and the wind direction, which is not important, since for all measurements the flight directions were chosen as up-, down-, and crosswind).

During former measurements with HELISCAT, no significant dependence of the damping behavior on water temperature was found (Hühnerfuss et al., 1994); thus, we assume that the measured differences of the damping behavior of OLA cannot be explained by the different water temperatures. Furthermore, also the air temperature should have no significant effect on the damping ratios (despite its impact on the NRCS, which is of no interest herein, since we have calculated ratios of the relative backscattered power).

No dependence of the damping ratios on the polarization of the microwaves was found, which is in accordance with the assumption made in the subsection Bragg Scattering that the Bragg coefficients should be independent of slick coverage [see Eq. (4)]. Moreover, we found no dependence of the damping ratios on the azimuth angle (i.e., the angle between antenna look direction and wind direction). Again, this is in accordance with other results obtained by HELISCAT (Hühnerfuss et al., 1994; 1996; Wismann et al., 1998; V. Wismann, personal communication, 1993). This effect can be explained, first, by means of the isotropy of the viscous damping (both on a slick-free and a slick-covered water surface). Second, other effects depending on the wind direction, like the energy input by the wind, are reduced in the presence of a slick. If we assume that this reduction does not depend on the azimuth angle, the measured damping ratios have to be independent of antenna look direction.

The damping ratios measured during the two experiments on 18 April 1994, at wind speeds of 5 m/s (Fig. 3) and 3.5–4 m/s (Fig. 4) are similar for low Bragg wavenumbers (k_B<80 rad/m). However, for intermediate to high Bragg wavenumbers a difference was observed: At 5 m/s wind speed (Fig. 3) the damping ratios are further (but less strong) monotonically increasing, whereas an abrupt increase at approximately 80 rad/m was measured at 3.5–4 m/s wind speed, in combination with a large scatter of the data (see Fig. 4).

One might suspect that instrumental parameters are responsible for this observation, that is, for the different wind dependence of the damping ratios for Bragg wavenumbers below and above 80 rad/m, respectively. The footprint size is the only parameter of the HELISCAT system which might affect the measurement results in

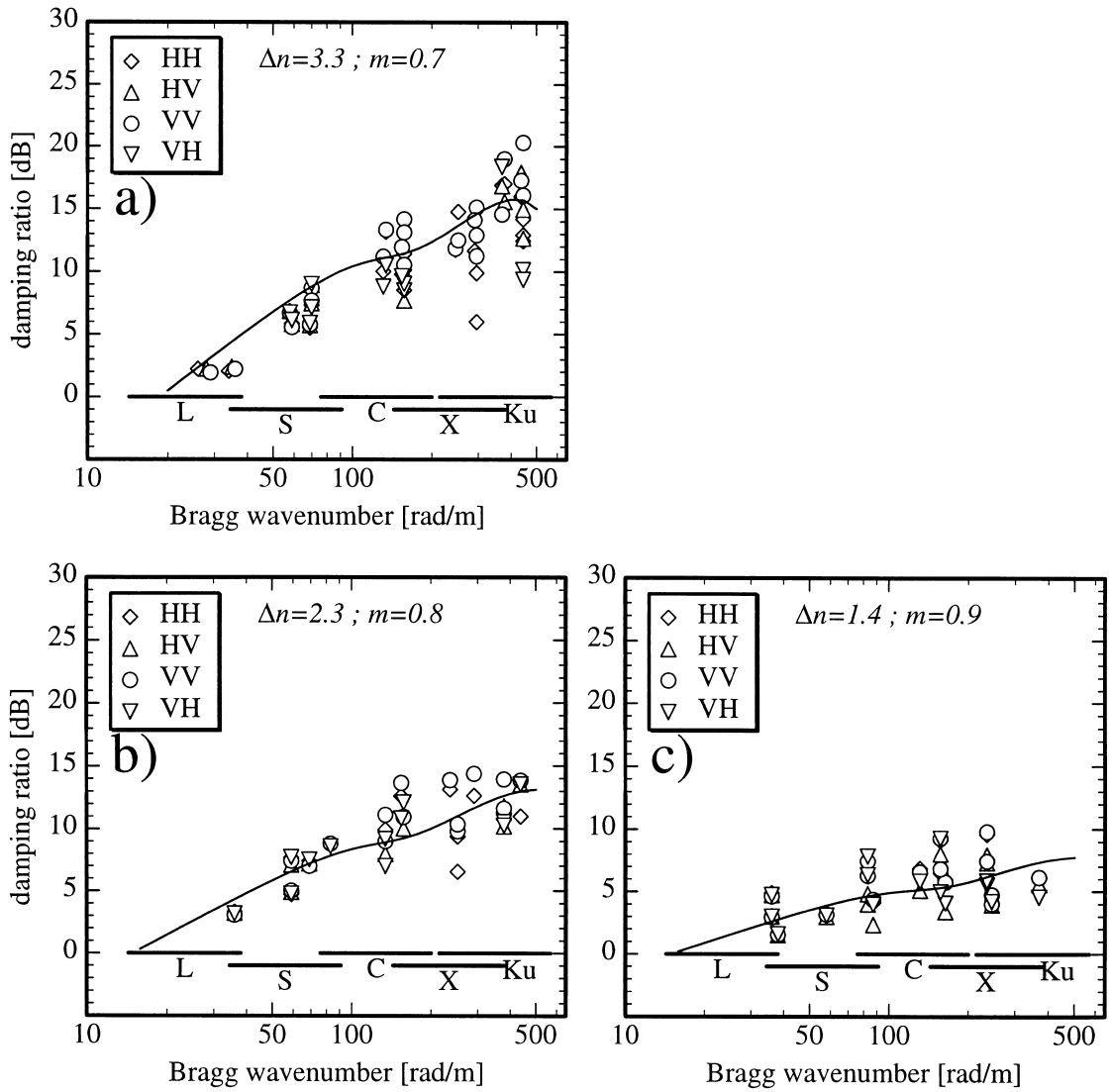

Figure 7. Same as Figure 5, but for pure TOLG. The data are subdivided into panel a: strong panel b: medium, and panel c: weak damping, corresponding to a maximum damping ratio of more than 15 dB, between 10 dB and 15 dB, and less than 10 dB, respectively.

such a way, since the dimensions of the footprint (at the same incidence angle) are decreasing with increasing radar frequency. If these dimensions were smaller than a certain limit, this could lead to the observed strong increase in the measured damping ratios. For example, the footprint dimensions for S band, at low incidence angle, are comparable with those for C band, at high incidence angle (approx. 22 m×10 m at S band, $\vartheta=23°$, and approx. 23 m×7 m at C band, $\vartheta=53°$, see Table 1). Thus, if a small footprint size would influence the data quality, it should be visible in Figure 4 both at 39 rad/m and at 177 rad/m (which are the corresponding Bragg wavenumbers for S band, $\vartheta=23°$, and C band, $\vartheta=53°$, respectively). However, since the large scatter was observed only at Bragg wavenumbers larger than 80 rad/m, we conclude that instrumental parameters (particularly the footprint dimensions) are not responsible for the measured peculiarities.

The damping ratios of OLA measured at wind speeds of 3.5–4 m/s, 5 m/s, and 12 m/s are shown in Figs. 4, 3, and 5, respectively. It can easily be seen that the damping ratios decrease with increasing wind speed, particularly at high Bragg wavenumbers (above 80 rad/m). This observation indicates that the wind speed has to be taken into account for the discussion of the obtained results. In order to allow a qualitative discussion of the measured results, the source terms for the wind input (at 4 m/s) and the viscous dissipation, both for a slick-covered water surface [divided by the spectral action density $N(k)$] are shown in Figure 10. The former, that is, the function β_s given in Eq. (8), was calculated setting $\varphi=0°$ and $u_*^{(s)}=0.7\cdot u_*^{(0)}=9.8$ cm/s. It can be inferred from Figure 10 that

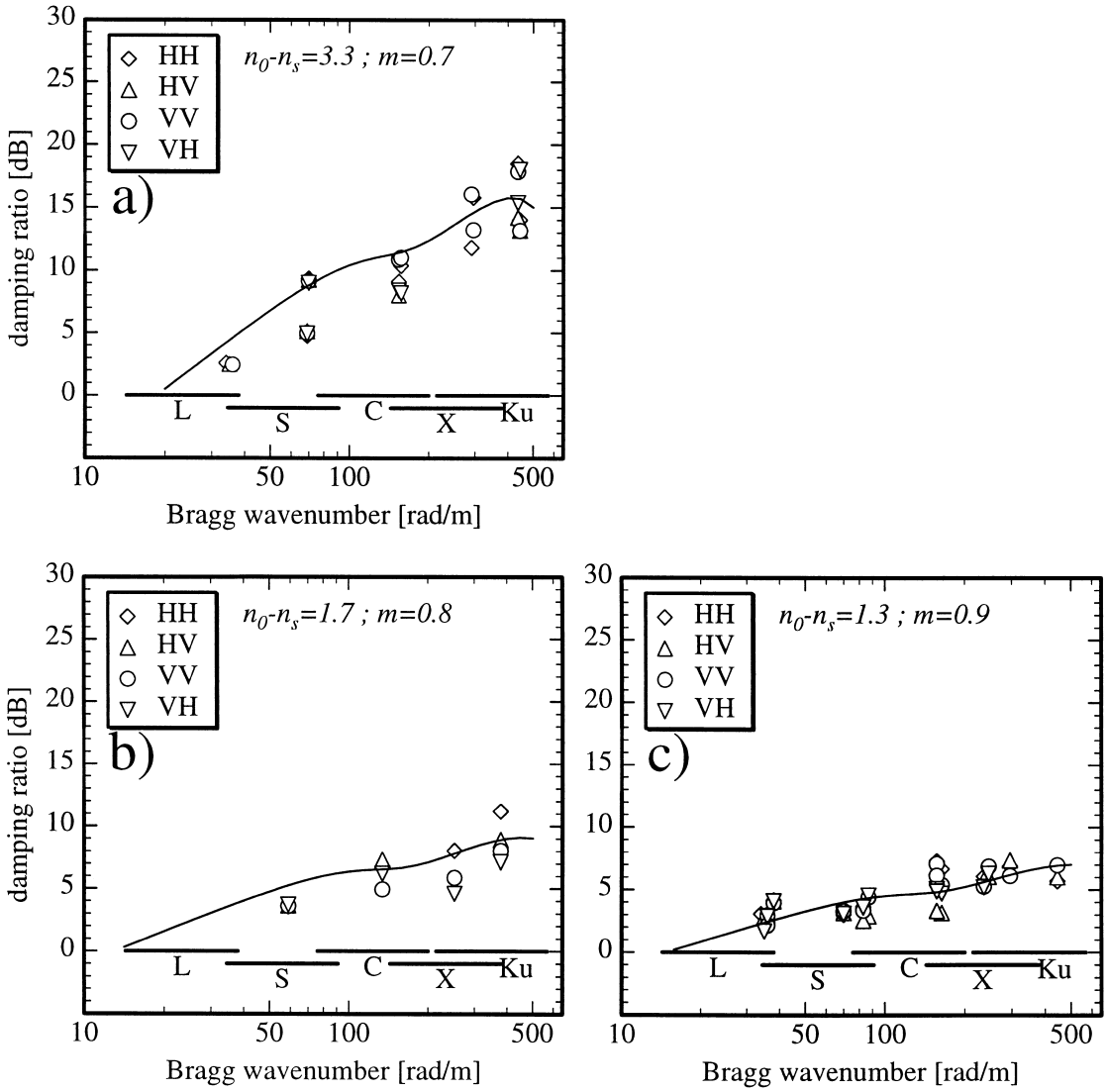

Figure 8. Same as Figure 7, but for TOLG dissolved in *n*-hexane.

only at low wavenumbers the energy input by the wind (dashed line) is larger than the viscous dissipation (solid line), whereas at intermediate to high wavenumbers the stronger viscous dissipation must result in high damping ratios.

It is worth noting that inserting the analytical expressions for these source terms into Eq. (10) gives rise to a singularity at the threshold wavenumber, that is, the wavenumber where both functions plotted in Figure 10, β_s and $2\Delta_s c_g$, are equal. Therefore, the calculation of theoretical damping ratios using Eq. (10) is sensible only for the high wind case, where the energy input by the wind is larger than the viscous dissipation for the whole wavenumber range which is of interest here.

For low wind speeds (and especially when the water surface is covered with a surface film), we may assume that wave breaking is not important; thus, for a balanced action [see Eq. (5)] nonlinear wave–wave interaction becomes important. The nonlinear energy flux must occur from low towards high wavenumbers (i.e., from wavenumbers lower than the threshold wavenumber towards those which are higher than this value; see Fig. 10). This in turn results in a wave damping at low wavenumbers stronger than predicted by Marangoni damping theory [as already mentioned by Alpers and Hühnerfuss (1989)]. Furthermore, at wavenumbers slightly higher than the threshold value, this energy flux may balance the lower energy input by the wind (in comparison to the viscous dissipation). However, in the wavenumber region of the Marangoni maximum (approx. 80 rad/m; see Fig. 2) the nonlinear energy flux may not be high enough to overcome the energy loss caused by the strong difference of viscous dissipation and wind input. We, therefore, expect a strong increase in the measured damping ratios in this wavenumber region, which in fact has been observed in our experiments.

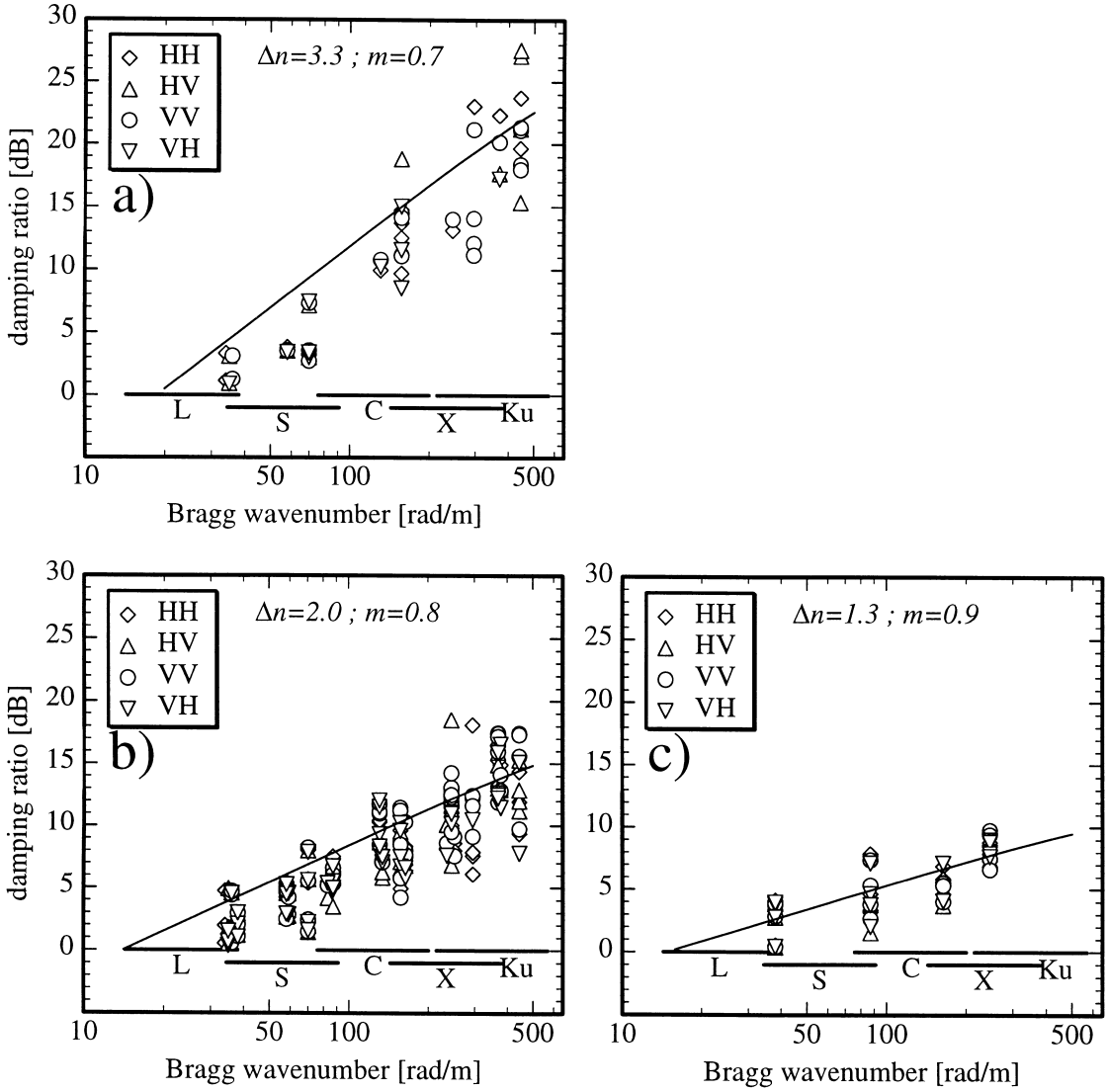

Figure 9. Same as Figure 7, but for the mineral oil (IFO 180).

At a wind speed of 5 m/s, the strong increase in the damping ratios at intermediate wavenumbers was not measured (see Fig. 3). Since the energy input by the wind at high wavenumbers and for this wind speed is still smaller than the viscous dissipation, another effect must be responsible for the monotonic increase of the measured damping ratios. During the first experiment on 18 April 1994, the direction of the tidal flow was antiparallel to the direction of the long wave propagation. Thus, the long waves should have been steeper, which in turn might cause a stronger wave breaking (particularly, on a slick-free water surface). We therefore suspect that the difference of viscous dissipation, on the one hand, and wind input and wave breaking, on the other hand, was not large enough to cause a strong increase in the measured damping ratios at intermediate Bragg wavenumbers (as measured at low wind speed).

During the third experiment on 6 October 1994, the wind speed was high (12 m/s) and the surface films were not coherent because of the permanent action of the waves and the strong wind. As described above, we therefore subdivided the data sets obtained from each of the surface films into classes of different (maximum) damping. The damping ratios for the four monomolecular surface films consisting of OLA, OLME, pure TOLG, and dissolved TOLG increase monotonically with Bragg wavenumber only for the "strong" damping parts of the slicks. The "weak" and "medium" damping parts, however, caused increasing damping ratios only at low Bragg wavenumbers (up to 80–150 rad/m, depending on the substance), whereas constant damping ratios were measured at high Bragg wavenumbers. This finding may be due to the fact that small holes in the slicks occurred locally. If short surface waves (i.e., waves with high Bragg wavenumbers) were generated within these holes by the wind, this in turn caused a reduction of the measured (mean) damping ratios.

It was already mentioned that only in the "strong"

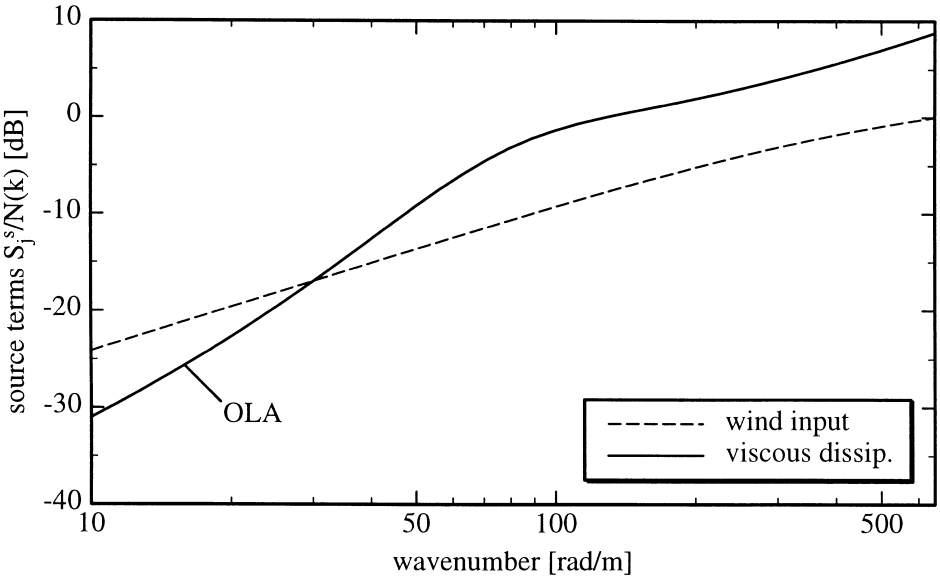

Figure 10. Wavenumber dependence of the factors of the source terms for wind input (dashed line) and viscous dissipation (solid line), β_s and Δ_s (as given in the section Basic Theory), respectively. For the wind input a wind speed of 4 m/s and a reduction of the friction velocity by 30% (with respect to the slick-free water surface) was assumed.

damping parts of the surface films a full coverage of the water surface by the different substances can be assumed. Therefore, the following comparison of the results obtained from the different surface films is restricted to the classes of "strong" damping, in order to avoid any influence on the data interpretation by tattered parts of the surface films.

For a qualitative analysis of the results measured at 12 m/s the source terms for the wind input and for the viscous dissipation are shown in Figure 11. The three dashed lines for the energy input by the wind were calculated assuming different reductions of the friction velocity over a slick-covered water surface (since classes of different damping were defined it is sensible also to assume different mean reductions of the friction velocity). It can easily be seen that (in contrast to the conditions at low to moderate wind speed; see Fig. 10) the energy input by the wind is larger than the viscous dissipation in the whole wavenumber range which is of interest in the present investigation. This can explain why no strong increase in the damping ratios at intermediate Bragg wavenumbers (approx. 80–150 rad/m) was measured. Furthermore, for a wind speed of 12 m/s, no singularity occurs in the first factor on the right-hand side of Eq. (10), so that a theoretical model of the damping ratios can be developed (see the next section).

As already measured at low to moderate wind speeds, the damping ratios from the "strong" damping parts of the OLA slick at 12 m/s (panel a of Fig. 5) are monotonically increasing with Bragg wavenumber. This increase, however, is smaller than measured during the two experiments in April 1994 at lower wind speeds (see Figs. 3 and 4). We can therefore infer that an increasing wind speed results in decreasing damping ratios, particularly

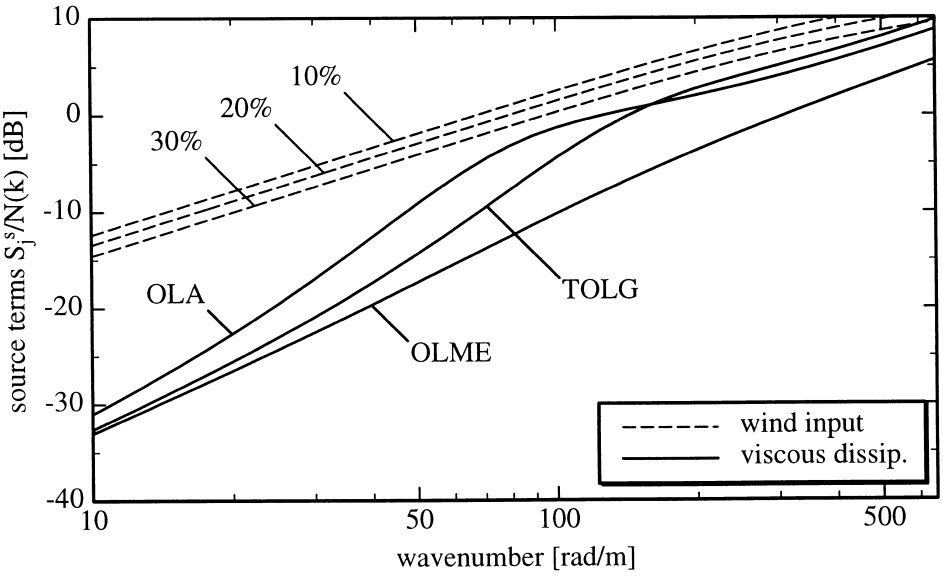

Figure 11. Same as Figure 10, but for a wind speed of 12 m/s. Three different reductions of the friction velocity were assumed (10%, 20%, and 30%), corresponding to the classes of different (mean) damping (see text).

at high Bragg wavenumbers, whereas the shape of the measured damping curves (i.e., the monotonic increase) is independent of wind speed. This finding can be explained by means of a stronger influence of the wind-dependent source terms in Eq. (10), that is, wind input and wave breaking, on the damping ratios, which results in a flattening of the measured damping curves.

The damping ratios measured at a wind speed of 12 m/s for the "strong" damping parts of the pure TOLG slick (panel a of Fig. 7) show similar properties as already measured for the different OLA slicks: We observed a monotonic increase with Bragg wavenumber and a slight kink at intermediate Bragg wavenumber. Again, the absence of a Marangoni maximum is a manifestation of the influence of the wind speed dependent source terms in Eq. (10). Up to Bragg wavenumbers of approximately 300 rad/m, the measured damping curves for the "strong" and "medium" damping parts of the pure TOLG slick are almost identical (see panels a and b of Fig. 7). Only at high Bragg wavenumbers (k_B>300 rad/m) were strong differences measured. As already mentioned, these differences may be due to small holes within the TOLG slick and, thus, a local generation of small surface waves (with wavelengths smaller than approx. 2 cm); however, they may also be due to the damping characteristics of the monomolecular surface films (see below).

Since the surface film consisting of dissolved TOLG was gradually destroyed during the measurements by the action of the strong wind and the waves, only a few data were obtained over this slick (see Fig. 8). Thus, less information can be inferred from this data set. However, the damping ratios measured over the "strong" damping part of the dissolved TOLG slick are similar to those measured over the "strong" damping part of the pure TOLG slick. This shows, that the different spreading procedure due to the solvent *n*-hexane has only a weak influence on the damping behavior of this substance (at least under high wind conditions). Differences between the data of the "medium" and "weak" damping parts of both TOLG slicks (panels b and c of Figs. 7 and 8) are apparently due to the different amount of data (particularly for the "medium" damping parts).

The damping ratios measured over the mineral oil spill consisting of IFO 180 (Fig. 9) show a monotonic increase for all damping classes, that is, not only for the areas of "strong" damping, but also for the "medium" and "weak" damping parts. For the "strong" damping parts of IFO 180, moreover, we measured the highest damping ratios observed during this experiment (at 12 m/s). For the "medium" and "weak" damping parts constant damping ratios at high Bragg wavenumbers (as measured over the monomolecular slicks) are absent. This may be a hint for the fact that this peculiarity is not only caused by small holes within the surface films, but that it is also due to the different damping characteristics of the different surface films.

The results reported herein are in accordance with those reported by Wismann et al. (1998; V. Wismann, personal communication, 1993) who also found, on the one hand, a monotonic increase in the damping ratios measured over mineral oils spills and, on the other hand, a less strong increase in the damping ratios (particularly at high Bragg wavenumbers) measured over monomolecular slicks. A different damping behavior of mineral oil spills was measured by Johnson and Croswell (1982) and by Singh et al. (1986), who both measured a reduction of the damping ratios at high Bragg wavenumbers (above 300 rad/m). However, since these particular data were obtained at incidence angles above 35° and, as in the case of Singh et al. (1986), at low to moderate wind speeds (3–6 m/s), we suspect that an insufficient signal-to-noise ratio was responsible for the measured reductions. Even the Ku band data from our measurements at low to moderate wind speeds (3.5–5 m/s) obtained at incidence angles above 40° could not be used in some cases, due to an insufficient signal-to-noise ratio, and were, therefore, omitted.

A Simple Model for the Measured Damping Ratios at High Wind Speeds (12 m/s)

The monotonic increase in the damping ratios already measured previously (Wismann et al., 1993) cannot be explained by pure Marangoni damping theory (see the theoretical damping curves shown in Fig. 2). Recently, attempts have been made to explain this discrepancy (Vesecky, 1995; Macklin, 1995). However, the experimental results could not fully be explained for the whole wind speed range for which the results had been obtained.

Under high wind conditions (above 10 m/s), the energy input by the wind is larger than the viscous dissipation in the whole (Bragg) wavenumber range covered by HELISCAT (i.e., up to approx. 600 rad/m). Since no singularities in the first factor on the right-hand side of Eq. (10) occur under these conditions, a model for the damping ratios can be developed.

For the source term for wave breaking Donelan and Pierson (1987) proposed a power-law behavior:

$$S_{br}=a(k^4\Phi(k))^n\omega N(k), \tag{11}$$

where a and n are functions of the wavenumber (depending on the kind of wave breaking) and had to be determined by fitting Eq. (11) to results from Ku band radar backscatter measurements. The spectral power density of the water waves, Φ, acts as an input spectrum into Eq. (11). For Φ Phillips (1985) proposed

$$\Phi(k)\propto\sqrt{\frac{|\cos\varphi|u_*^2}{gk^7}}. \tag{12}$$

Inserting Eq. (12) into Eq. (11), setting the function n constant as n=3, and using Eq. (3), we obtain a result

which is in accordance with an expression for spontaneous breaking proposed by Phillips (1988).

Let us now assume that the function n (and, thus, the kind of breaking) depends on the slick coverage of the water surface. Furthermore, let us assume that, under high wind conditions and in the wavenumber range which is of interest herein, the source terms for the nonlinear wave–wave interaction are negligible in comparison to the source terms of wave breaking (Donelan and Pierson, 1987). The second factor on the right-hand side of Eq. (10) can then be written as

$$\frac{S_{nl}^0 - S_{br}^0}{S_{nl}^s - S_{br}^s} \approx A(\varphi, n_0, n_s) \cdot k^{(n_0 - n_s)/2} \tag{13}$$

with

$$A(\varphi, n_0, n_s) \propto \frac{a_0}{a_s} \cdot m^{-n_s - 1} \cdot u_*^{n_0 - n_s} \left(\sqrt{\frac{|\cos \varphi|}{g}} \right)^{n_0 - n_s},$$

where n_0 and n_s denote the function n in Eq. (11) for a slick-free and slick-covered water surface, respectively, and m denotes the reduction of the friction velocity by the slick, that is, $u_*^{(s)} = m \cdot u_*^{(0)}$. Let us assume that the function A only depends on the azimuth angle φ and on n_0 and n_s, i.e., the ratio a_0/a_s may be independent of wavenumber.

Donelan and Pierson (1987) expressed a as an exponential function with exponent n. For simplicity, we thus may assume that $a = 2^n$, where n is a constant number which is reduced in the presence of a slick (i.e., the waves are less breaking). We, therefore, may set

$$\frac{a_0}{a_s} = 2^{\Delta n}, \tag{14}$$

with $\Delta n = n_0 - n_s$. Inserting Eqs. (13) and (14) into Eq. (10) and setting $n_0 = 3$, which is in accordance with Phillips (1988), we obtain a simple expression for the wind-speed-dependent damping ratio:

$$\frac{\sigma^{(0)}(k)}{\sigma^{(s)}(k)} = \frac{\Psi_0(k)}{\Psi_s(k)} \approx \frac{\beta_s - 2\Delta_s c_g}{\beta_0 - 2\Delta_0 c_g} \cdot m^{\Delta n - 4} \left(2u_* \cdot \sqrt{\frac{|\cos \varphi| k}{g}} \right)^{\Delta n}, \tag{15}$$

where the factors of the source terms of wind input (β_i) and viscous dissipation (Δ_i) are given in the section Basic Theory.

Under high wind speed conditions, the wind-induced effects (i.e., the energy input by the wind and the wave breaking) are dominating in Eq. (15), thus resulting in a power-law function for the theoretical damping ratios. This, in turn, yields a linear curve in the double-logarithmic domain, where the slope of this curve depends primarily on the reduction of the wave breaking; that is, a strong reduction of the wave breaking results in a steep slope of the damping curve, and vice versa. For a weak reduction of the wave breaking (i.e., for small values of Δn) the first factor on the right-hand side of Eq. (15) dominates, which results in a small slope of the damping curve and, due to the Marangoni damping, in a flattening of the damping curve at high Bragg wavenumbers. These predictions are in qualitative agreement with the results of our measurements presented above.

By varying the parameters m and Δn in Eq. (15) describing the reduction of the friction velocity and of the wave breaking, respectively, theoretical damping curves have been calculated as best fit to the experimental data (the exact values of m and Δn were calculated by applying a least-square method). Since no significant dependence on the antenna look direction relative to the wind direction was found in our results, the azimuth angle φ was set equal to zero for all simulations [it is obvious that a less strong dependence of the wave spectrum on the azimuth angle than proposed in Eq. (12) is required (Donelan and Pierson, 1987)].

For the "strong," "medium," and "weak" damping parts of all surface films, the reduction factor for the friction velocity, m, was set equal to 0.7, 0.8, and 0.9, respectively, corresponding to a different energy input by the wind (see Fig. 11). The modeling results for OLA are inserted as solid lines into Figure 5. The monotonic increase of the damping ratios measured for the "strong" and "medium" damping parts (panels a and b, respectively) could successfully be modeled, setting the parameter for the reduction of the wave breaking, Δn, equal to 3.3 and 2.4, respectively. Note that the modeling results show no maximum at intermediate (Bragg) wavenumbers as would be the case for pure Marangoni damping (Fig. 2). The measured damping ratios obtained from the "weak" damping parts of the OLA slick (panel c) could be modeled by setting $\Delta n = 1.8$, that is, a smaller value for the reduction of the wave breaking was chosen than for the "strong" and "medium" damping parts, which is in accordance with the qualitative discussion above. It is, thus, obvious that the model is also capable of simulating lower damping ratios for the same substance by decreasing the two parameters for the reduction of the friction velocity and the wave breaking.

The modeling results for the other monomolecular slicks consisting of OLME, pure TOLG, and dissolved TOLG are also inserted as solid lines into Figures 6, 7 and 8, respectively. In all cases, the monotonic increase in the theoretical curves for the "strong" damping parts (panels a) corresponds to the results of our measurements. In particular, the Marangoni maximum for TOLG (see Fig. 2) causes a less increasing theoretical curve in that particular wavenumber range, which is in agreement with our results.

Finally, the modeling results for the mineral oil spill consisting of IFO 180 are inserted as solid lines in Figure 9. For the mineral oil, pure viscous damping was assumed using Eq. (6) and inserting the dynamic viscosity of IFO 180, $\eta = 0.002$ Pa s. Most notable is the fact that the monotonic increase, which was measured not only for the "strong" damping parts (panel a), but also for the

"medium" and "weak" damping parts (panels b and c, respectively), could well be reproduced. In particular, inserting lower values for the parameters Δn and m into Eq. (15) does not cause a flattening of the modeled curves, as obtained for the monomolecular slicks. Thus, using Eq. (15) we can explain, on the one hand, that only slight qualitative differences between the artificial quasibiogenic and anthropogenic surface films were measured over the "strong" damping parts and, on the other hand, that a different qualitative damping behavior was observed over the "medium" and "low" damping parts.

Our model shows a strong dependence on the azimuth angle φ, which is due to fact that only simple assumptions were made for this dependence both for the wind input [Eq. (8)] and the wave spectrum [Eq. (12)]. It was already mentioned (see, e.g., Donelan and Pierson, 1987; Phillips, 1988) that a parametrized (i.e., weaker) dependence should be chosen in order to get more realistic results, particularly, for the azimuthal dependence of the wave spectrum. However, a variation of the azimuth angle in Eq. (15) by $\pm 30°$ does not cause significant changes of the qualitative results, that is, by slightly increasing the parameter Δn, similar damping curves can be calculated for all surface films (not shown herein). Moreover, for the "weak" damping parts (and for all damping parts of substances which show an overall low damping behavior, like OLME), the azimuth angle in Eq. (15) can be varied to a much higher extent ($\pm 60°$). Thus, if we assume a less strong dependence on the azimuth angle, our model can also explain why no significant dependence on the antenna look direction was observed.

The results of the theoretical model developed herein are, therefore, capable of explaining the observations made in our experiments at high wind speed (12 m/s), for example, the similarities measured for the different kinds of surface films (particularly, the monotonic increase in the damping ratios for the "strong" damping parts) and the similar amount of wave damping caused by the different types of surface films. However, it is not applicable to lower wind speeds ($U_{10}<10$ m/s), where also nonlinear wave–wave interaction has to be taken into account.

SUMMARY AND CONCLUSIONS

During the two SIR-C/X-SAR missions in April and October 1994, three surface film experiments were performed in the German Bight of the North Sea, in order to investigate the reduction of the radar backscatter from the ocean surface by different oceanic surface films. For this purpose, radar backscatter measurements were carried out with the 5-frequency/multipolarization scatterometer HELISCAT of the University of Hamburg at L, S, C, X, and Ku band. During all measurements, monomolecular slicks consisting of oleyl alcohol (OLA) were deployed, thus allowing for an investigation of the dependence of the damping behavior on different environmental conditions, in particular, on wind speed.

It was found that, under all wind speed conditions (3.5–5 m/s in April 1994 and 12 m/s in October 1994), the measured damping ratios (i.e., the ratios of the radar backscatter from a slick-free and a slick-covered water surface) for all surface films increase with increasing Bragg wavenumber. However, at high wind speed (12 m/s), those parts of the monomolecular surface films which may have partly been destroyed by the continuous action of the strong wind ("medium" and "weak" damping parts), cause constant damping ratios at high Bragg wavenumbers (above approx. 100 rad/m).

The observed damping behavior of the monomolecular surface films cannot be explained by pure Marangoni damping theory which describes the damping of small sinusoidal water surface waves by monomolecular slicks and which predicts a distinct damping maximum at intermediate wavenumbers of approximately 100 rad/m. Additionally, wind-induced effects, primarily the energy input into the wave spectrum, have to be considered.

The damping ratios measured for the OLA slicks at low to moderate wind speed (3.5–4 m/s and 5 m/s) are qualitatively explained by taking into account the different source terms of the action balance equation. Here the difference between the wind input and the viscous dissipation, on the one hand, and the nonlinear wave–wave interaction, on the other hand, were adequately included.

For the high wind speed case (12 m/s, where the energy input by the wind is larger than the viscous dissipation in the whole Bragg wavenumber range), a theoretical model for the damping ratio was developed. This model can well reproduce the measured damping ratios and, moreover, the absence of the expected Marangoni damping maximum at intermediate Bragg wavenumbers (approx. 100 rad/m) can be interpreted. Furthermore, the model can explain the similarities between the results obtained from quasibiogenic and anthropogenic surface films under high wind conditions.

During the two SIR-C/X-SAR missions in April and October 1994, SAR images were acquired over the same surface films (deployed west of the island of Sylt) which were overflown by HELISCAT. The damping ratios obtained from these SAR images have recently been presented by Gade et al. (1998b). It is remarkable that, over each surface film, SIR-C/X-SAR measured lower damping ratios than HELISCAT [see Figs. 4 and 9 in Gade et al. (1998b)], whereas these differences are increasing with Bragg wavenumber. For the second shuttle mission, this observation is even more surprising, since the HELISCAT measurements were performed 2 h after the SAR image acquisition (therefore, the damping capability of OLA should have been reduced due to the action of the waves and the strong wind). It is noteworthy that both sensors measured similar differences between the

results obtained from both OLA slicks (corresponding to the two surface film experiments). Possible explanations for this finding may include different resolution scales (25 m for the SAR system, for the footprint dimensions of the HELISCAT systems see Table 2), while time differences and state of evolution of the slick in our opinion play a minor role. Additional systematic investigations are required in order to answer these questions.

The authors would like to thank the members of the Special Federal Unit for Marine Pollution Control (SBÖ), particularly Capt. Schroh, for their help in organizing the experiments and the recovery of the mineral oil. Special thanks are due to the helicopter crews, particularly to U. Lahrmann and O. Hillebrandt, of Helicopter Service Wasserthal, Hamburg, for their engaged collaboration. We also wish to thank H. Dannhauer, V. Neumann, J. Simon-Kutscher, R. Gatermann, and the vessel crews (particularly Capt. Röw and Capt. Jakobs) for their help during the experiments. We are grateful to R. Franck for his engaged help in processing the HELISCAT data. This work has been supported by the German Space Agency (DARA) under Contract 01QS9016/50QS90165 and by the German Science Foundation (DFG) under Contract Hu583/1-2.

REFERENCES

Alpers, W. (1995), Measurement of mesoscale oceanic and atmospheric phenomena by ERS-1 SAR. *URSI Radio Sci. Bull.* 275:14–22.

Alpers, W., and Hühnerfuss, H. (1988), Radar signatures of oil films floating on the sea and the Marangoni effect. *J. Geophys. Res.* 93:3642–3648.

Alpers, W., and Hühnerfuss, H. (1989), The damping of ocean waves by surface films: a new look at an old problem. *J. Geophys. Res.* 94:6251–6265.

Alpers, W., Wismann, V., Theis, R., et al. (1991), The damping of ocean surface waves by monomolecular sea slicks measured by airborne multi-frequency radars during the SAXON-FPN experiment. In *Proc. Int. Geosci. and Remote Sens. Symp.* (*IGARSS*), *11*, Espoo, Finland, pp. 1987–1990.

Bentz, A. P. (1980), Oil spill identification and remote sensing. In *Petroleum in the Marine Environment* (L. Petrakis and F. Weis, Eds.), Adv. Chem. 185, American Chemical Society, Washington, DC, pp. 22–86.

Cini, R., and Lombardini, P. P. (1978), Damping effect of monolayers on surface wave motion in a liquid. *J. Colloid Interface Sci.* 65:387–389.

Donelan, M. A., and Pierson, W. J. (1987), Radar scattering and equilibrium ranges in wind-generated waves with application to scatterometry. *J. Geophys. Res.* 92:4971–5029.

Ermakov, S. A., Zujkova, E. M., Panchenko, A. R., Salashin, S. G., Talipova, T. G., and Titov, V. I. (1986), Surface film effect on short wind waves. *Dyn. Atmos. Oceans* 10:31–50.

Frysinger, G. S., Asher, W. E., Korenowski, G. M., et al. (1992), Study of ocean slicks by nonlinear laser processes 1. second-harmonic generation. *J. Geophys. Res.* 97: 5253–5269.

Gade, M. (1996), Untersuchungen zur Abbildung biogener und anthropogener Oberflächenfilme auf dem Meer mit Hilfe von Radarsensoren, Ph.D. thesis, University of Hamburg, Department of Geosciences, Hamburg, Germany; Shaker, Aachen, 170 pp.

Gade, M., Alpers, W., Hühnerfuss, H., and Lange, P. A. (1998a), Wind wave tank measurements of wave damping and radar cross sections in the presence of monomolecular surface films. *J. Geophys. Res.* 103:3167–3178.

Gade, M., Alpers, W., Hühnerfuss, H., Masuko, H., and Kobayashi, T. (1998b), Imaging of biogenic and anthropogenic ocean surface films by the multifrequency/multipolarization SIR-C/X-SAR. *J. Geophys. Res.*, in press.

Gade, M., Alpers, W., Ermakov, S. A., Hühnerfuss, H., and Lange, P. A. (1998c), Wind wave tank measurements of bound and freely propagating short gravity capillary waves. *J. Geophys. Res.*, in press.

Hasselmann, K. (1962), On the nonlinear energy transfer in a gravity wave spectrum, 1: General theory. *J. Fluid Mech.* 12:481–500.

Hasselmann, K. (1963a), On the nonlinear energy transfer in a gravity wave spectrum, 2: Conservation theorems, wave-particle analogy, irreversibility. *J. Fluid Mech.* 15:273–281.

Hasselmann, K. (1963b), On the nonlinear energy transfer in a gravity wave spectrum, 3: Evaluation of the energy flux and swell-sea interaction for a Newmann spectrum. *J. Fluid Mech.* 15:385–398.

Hühnerfuss, H. (1986), The molecular structure of the system water/monomolecular surface film and its influence on water wave damping, Habilitationsschrift, University of Hamburg, Department of Chemistry, Hamburg, Germany, 245 pp.

Hühnerfuss, H., and Garrett, W. D. (1981), Experimental sea slicks: their practical applications and utilization for basic studies of air-sea interactions. *J. Geophys. Res.* 86:439–447.

Hühnerfuss, H., Lange, P. A., and Walter, W. (1982), Wave damping by monomolecular surface films and their chemical structure. Part I: Variation of the hydrophobic part of carboxylic acid esters. *J. Mar. Res.* 40:209–225.

Hühnerfuss, H., Gericke, A., Alpers, W., Theis, R., Wismann, V., and Lange, P. A. (1994), Classification of sea slicks by multifrequency radar techniques: new chemical insights and their geophysical implications. *J. Geophys. Res.* 99:9835–9845.

Hühnerfuss, H., Alpers, W., Dannhauer, H., et al. (1996), Natural and man-made sea slicks in the North Sea investigated by a helicopter-borne 5-frequency radar scatterometer. *Int. J. Remote Sens.* 17:1567–1582.

Hunter, K. A. and Liss, P. S. (1981), Organic sea surface films. In *Marine Organic Chemistry: Evolution, Composition, Interactions and Chemistry of Organic Matter in Sea Water* (E. K. Duursma and R. Dawson, Eds.), Elsevier, Amsterdam.

Johnson, J. W., and Croswell, W. F. (1982), Characteristics of 13.9 GHz radar scattering from oil films on the sea surface. *Radio Sci.* 17:611–617.

Lombardini, P. P., Fiscella, B., Trivero, P., Cappa, C., and Garrett, W. D. (1989), Modulation of the spectra of short gravity waves by sea surface films: slick detection and characterization with a microwave probe. *J. Atmos. Ocean. Technol.* 6:883–890.

Lucassen, J. (1982), Effect of surface-active material on the damping of gravity waves: a reappraisal. *J. Colloid Interface Sci.* 85:52–58.

Lucassen-Reynders, E. H., and Lucassen, J. (1969), Properties of capillary waves. *Adv. Colloid Int. Sci.* 2:347–395.

Macklin, J. T. (1995), Modelling of the visibility of sea-surface films in radar images as a function of wind speed. In *Proc. Int. Geosci. Remote Sens. Symp. (IGARSS), 15,* Florence, Italy, pp. 1367–1368.

Melsheimer, C., Alpers, W., and Gade, M. (1998), Investigation of multifrequency/multipolarization radar signatures of rain cells, derived from SIR-C/X-SAR data. *J. Geophys. Res.* in press.

Mitsuyasu, H., and Honda, T. (1982), Wind-induced growth of water waves. *J. Fluid Mech.* 123:425–442.

Okamoto, K., Masuko, H., Ochiai, S., et al. (1993), Artificial oil pollution detection and wave observation in the sea adjacent to Japan by ERS-1 SAR. In *Proc. 1st ERS-1 Symp.* Cannes, France, 1992, pp. 817–821.

Onstott, R., and Rufenach, C. (1992), Shipboard active and passive microwave measurement of ocean surface slicks off the southern California coast. *J. Geophys. Res.* 97:5315–5323.

Pellemans, A. H. J. M., Bos, W. G., Konongs, H., and van Swol, R. W. (1995), Oil spill detection on the North Sea using ERS–1 SAR data, BCRS Report 94–30, Netherlands Remote Sensing Board (BCRS), Delft, The Netherlands.

Phillips, O. M. (1977), *The Dynamics of the Upper Ocean*, 2nd ed., Cambridge University Press, New York, 336 pp.

Phillips, O. M. (1985), Spectral and statistical properties of the equilibrium range in wind-generated gravity waves. *J. Fluid Mech.* 156:505–531.

Phillips, O. M. (1988), Radar returns from the sea surface—Bragg scattering and breaking waves. *J. Phys. Ocean.* 18: 1065–1074.

Plant, W. J. (1982), A relationship between wind stress and wave slope. *J. Geophys. Res.* 87:1961–1967.

Singh, K. P., Gray, A. L., Hawkins, R. K., and O'Neil, R. A. (1986), The influence of surface oil on C- and Ku-band ocean backscatter. *IEEE Trans. Geosci. Remote Sens.* GE–24:738–744.

Valenzuela, G. R. (1978), Theories for the interaction of electromagnetic and oceanic waves—a review. *Boundary Layer Meteorol.* 13:61–85.

Vesecky, J. (1995), Surface film effects on the radar cross section of the ocean surface. In *Proc. Int. Geosci. and Remote Sens. Symp.* (*IGARSS*), *15*, Florence, Italy, pp. 1375–1377.

Wahl, T., Anderssen, T., and Skøelv, Å. (1994), Oil spill detection using satellite based SAR; pilot operation phase, final report, Norwegian Defense Research Establishment (internal report).

Wei, Y., and Wu, J. (1992), In situ measurements of surface tension, wave damping, and wind properties modified by natural films. *J. Geophys. Res.* 97:5307–5313.

Wismann, V., Theis, R., Alpers, W., and Hühnerfuss, H. (1993), The damping of short gravity-capillary waves by experimental sea slicks measured by an airborne multi-frequency scatterometer, In *Proc. Oceans'93*, Vol. II, Vancouver, Canada, pp. 342–347.

Wismann, V., Gade, M., Alpers, W., and Hühnerfuss, H. (1998), Radar signatures of marine mineral oil spills measured by an airborne multifrequency radar. *Int. J. Remote Sens.* in press.

Wright, J. W. (1968), A new model for sea clutter. *IEEE Trans. Antennas Propagation* AP-16:217–223.

Wu, J. (1975), Wind induced drift currents. *J. Fluid Mech.* 68:49–70.

Wu, J. (1989), Suppression of oceanic ripples by surfactant-spectral effects deduced from sun-glitter, wave-staff and microwave measurements. *J. Phys. Oceanogr.* 19:238–245.